Structural Engineering and Mechanics, *Vol. 57, No. 2 (2016) 327-355*
DOI: http://dx.doi.org/10.12989/sem.2016.57.2.327

Elastic solutions due to a time-harmonic point load in isotropic multi-layered media

Gao Lin[1a], Pengchong Zhang[1b], Jun Liu[*1,2,3] and Wenyuan Wang[1c]

[1]*School of Hydraulic Engineering, Faculty of Infrastructure Engineering, Dalian University of Technology, Dalian 116024, China*
[2]*State Key Laboratory of Structural Analysis for Industrial Equipment, Dalian University of Technology, Dalian 116024, China*
[3]*State Key Laboratory of Ocean Engineering, Shanghai Jiao Tong University, Shanghai 200240, China*

(Received July 25, 2015, Revised December 24, 2015, Accepted December 28, 2015)

Abstract. A new analytical derivation of the elastodynamic point load solutions for an isotropic multi-layered half-space is presented by means of the precise integration method (PIM) and the approach of dual vector. The time-harmonic external load is prescribed either on the external boundary or in the interior of the solid medium. Starting with the axisymmetric governing motion equations in a cylindrical coordinate system, a second order ordinary differential matrix equation can be gained by making use of the Hankel integral transform. Employing the technique of dual vector, the second order ordinary differential matrix equation can be simplified into a first-order one. The approach of PIM is implemented to obtain the solutions of the ordinary differential matrix equation in the Hankel integral transform domain. The PIM is a highly accurate algorithm to solve sets of first-order ordinary differential equations and any desired accuracy of the dynamic point load solutions can be achieved. The numerical simulation is based on algebraic matrix operation. As a result, the computational effort is reduced to a great extent and the computation is unconditionally stable. Selected numerical trials are given to validate the accuracy and applicability of the proposed approach. More examples are discussed to portray the dependence of the load-displacement response on the isotropic parameters of the multi-layered media, the depth of external load and the frequency of excitation.

Keywords: time-harmonic point load; precise integration method; Hankel integral transform; dual vector; stratified soil

1. Introduction

The estimation for the magnitude and distribution of the displacements and stresses in the homogenous isotropic multi-layered soil has been a hot topic in soil and rock mechanics for a long

∗Corresponding author, Lecturer, E-mail: liujun8128@126.com
[a]Professor, E-mail: gaolin@dlut.edu.cn
[b]Ph.D., E-mail: zhangpengchong2014@126.com
[c]Ph.D. Student, E-mail: wangwenyuan@dlut.edu.cn

Copyright © 2016 Techno-Press, Ltd.
http://www.techno-press.org/?journal=sem&subpage=8 ISSN: 1225-4568 (Print), 1598-6217 (Online)

time. The solutions may contribute greatly to the design of structures such as pile foundations, municipal pipelines and metro tunnels. From the stand point of engineering applications, the media is often assumed to be homogeneous, isotropic and linearly elastic. Moreover due to a geologic process of sedimentation over a long period of time, soil in geotechnical engineering is always multi-layered. Therefore, in order to gain a more exact result for the practical engineering, it is essential and significant to study the field of displacements and stresses in the multi-layered isotropic materials. The distributions of stresses and displacements due to the action of the external forces concentrated at a point either on the boundary surface or in the interior of the elastic multi-layered region are known as point load solutions. It is worth to point out that the point load solutions can be taken as fundamental solutions to solutions of the complex loading problems. What's more, the point load solutions can be used to construct solutions for the analytical examination of the elastic problems and incorporated into numerical schemes such as boundary element method. The research on the point load solutions in academia is so important that numerous researchers are concerned with this issue.

Classical studies related to point load solutions in a homogeneous elastic infinite space were given by Kelvin (1848) and in a semi-infinite space by Boussinesq (1885) with the load on the surface of the half-space. Lamb (1901) proposed a perfectly simple and straightforward method to acquire the displacement response in an isotropic half-space under pressures applied normally to the free surface. Mindlin (1939) firstly studied the response of the elastic half-space subjected to a point load which was in the interior of the medium and created Mindlin's solution. Burmister (1945) focused on the general theory of stresses and displacements in a two-layered and three-layered system to facilitate the airport and foundation engineering. Rongved (1955) solved the problem of a point load acting in the interior of two joined semi-infinite media by introducing Papkovitch potential functions. Plevako (1969) derived the solutions for the deformation field caused by the concentrated load acting in the interior of two-layered half-space with different material properties. Harding and Sneddon (1945) studied the axisymmetric elastostatic problems of the homogeneous half-space using the integral transform technique (Sneddon 1951, 1972). Burmister (1956) made a further research on the displacement and stress solutions for the two-layered soil with the bottom fixed under a point load on the plane boundary. Muki (1960) generalized the Harding and Sneddon's approach to solve the asymmetric problems. Gilbert and Backus (1966) took advantage of the propagator matrix method to demonstrate the analysis of wave propagation in layered media. Bufler (1971) conducted a formal and exact solution to the distribution of stresses and displacements in a multilayered medium making use of integral transform technique and matrix analysis. With the aid of integral transform technique, Chan *et al*. (1974) formulated the solution for a two-layered semi-infinite domain caused by a vertical or horizontal point load applied in the interior of the system. Davies and Banerjee (1978) presented infinite series solutions of displacements in both layers of a two-layered half-space subjected to the horizontal and vertical point loads at the layer interface. Kausel and Peek (1982) revealed closed-form dynamic Green's functions based on a discretization of the medium in the layering direction. Luco and Apsel (1983) studied the response of a multi-layered half space and viscoelastic media subjected to a time-harmonic buried source. Benitez and Rosakis (1987) utilized the two-dimensional Fourier transform method and the transfer matrices approach to discuss the exact state of stresses and displacements in an infinite three-dimensional layer under concentrated body forces acting on an arbitrary internal point. Using the method of a mixed finite element, Stolle (1989) introduced a two-dimensional axisymmetric model to analyze the interaction between a static axisymmetric load and a layered pavement structure. According to Nat, Sarva and Sunita (1992),

the static displacement and stress field for a stratified elastic medium subjected to symmetric and asymmetric loads with the technique of transfer matrix was investigated. Yue (1995) conducted a study on the generalized Kelvin's problems of a multilayered medium due to concentrated forces by applying classical integral transforms and a backward transfer matrix method and proposed point load solutions to the layered elastic materials of infinite lateral extent, where the number of dissimilar elastic layers can be an arbitrary integer. Selvadurai (2001) showed the detailed derivation to obtain the solution of Boussinesq's problem with a concentrated normal load on the surface of an isotropic elastic half-space. Yue *et al*. (1995) illustrated the variations of stresses and displacements under an external point load in a two-layered soil, where the elastic parameters of geo-materials are variable with depth. Employing axisymmetric governing equations, Hankel's transform and matrix analysis, the paper (Wang and Ishikawa 2001) was concerned with the distribution of stresses and displacements in a linearly elastic multi-layered medium under axisymmetric load. Ai *et al*. (2002) generalized Sneddon and Muki solutions and applied the transfer matrix method to solve elastostatic problems of the multilayered materials. Zhang and Li (2011) utilized the integral transform and the transfer matrix technique to determine the field of stresses and displacements in the elastic layered geo-materials subjected to an arbitrary point load in the Cartesian coordinate system. Futoshi *et al*. (2013) presented stress and strain responses in terms of a volumetric strain for an elastic multilayered structure under uniform and non-uniform loads. Chen (2015) studied the time-harmonic vibrations of a rigid circular foundation resting on a multi-layered elastic half-space. With the aid of the continued fraction solution, Lu *et al*. (2015) proposed a modified scaled boundary element method in the time domain to simulate the unbounded domain with bedrock.

As a semi-analytical technique to solve the partial differential equations (Song and Wolf 1997, 2000, Wolf 2003), the scaled boundary finite-element method (SBFEM), which only needs to discretize the boundary and is no need for the fundamental solution, also can be applicable to the multilayered medium. Genes *et al*. (2005) were the earliest researchers who paid attention to combining finite element method (FEM), boundary element method (BEM) and scaled boundary finite element method (SBFEM) to acquire the dynamic response of 2D structures resting on layered media. However, the coupled model can not simulate the infinite lateral extent precisely. A modified scaled boundary finite element method (Birk and Behnke 2012) with degenerating the original scaling centre into the scaling line can solve the soil structure interaction in the layered system. But this operation is only suitable for the issue of a layered soil depositing over rigid bedrock. Chen *et al*. (2012) introduced a kind of time domain analysis using the technique of displacement unit-impulse response matrix for the layered media.

The objective of this paper is to present a novel method to obtain the solutions of displacements and stresses in the stratified medium under a point load. The concentrated force may be prescribed either at the external surface or within the multilayered materials. In the process, the key ordinary differential equations are evaluated by the precise integration method (PIM) (Zhong *et al*. 2004). Making use of the Hankel integral transform, a second order ordinary differential matrix equation can be gained from the axisymmetric wave motion equations in a cylindrical coordinate system. Employing a couple of dual vectors about displacements and stresses, the second order ordinary differential matrix equation can be simplified into a first-order one. Utilizing the approach of PIM, the solutions to the ordinary differential matrix equation in the Hankel integral transform domain for the continuum subjected to a vertical point load can be known. In order to get the solutions in physical space domain, it is essential to take the Hankel inverse transform. As the Bessel functions generally can't be carried out in exact closed forms, a numerical quadrature technique usually has

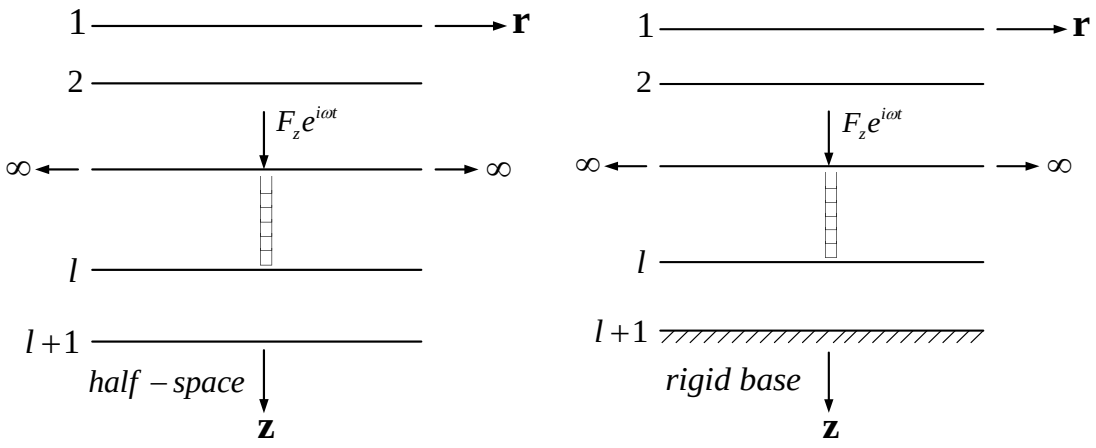

Fig. 1 Multi-layered soil model (a) resting on half-space (b) fixed base

to be adopted in such evaluations. Numerical trials are provided to check the effectiveness and accuracy of the proposed procedure. It is found that the numerical results and the exact solutions are in good correspondence. Further, more examples are given to depict the generalization of the proposed procedure and the effect of material parameters on the point solutions.

2. Fundamental derivation

Consider a set of linearly elastic, parallel layers of infinite horizontal extent as shown in Fig. 1. The load may be either applied on the surface of the soil or at the interface between the stratums. The origin of the cylindrical coordinate system is set on the surface with the z-axis in the depthwise direction with respect to the horizontal interface of the domain and it is the common axis of symmetry of the solid as illustrated in Fig. 1.

The axisymmetric governing equations of time-harmonic motion for a homogeneous isotropic elastic continuum in terms of displacements and in the absence of body forces in a cylindrical coordinate system can be expressed as

$$d_{11}\left(\nabla^2 u_r - \frac{u_r}{r^2}\right) + d_{44}\frac{\partial^2 u_r}{\partial z^2} + \left(d_{13}+d_{44}\right)\frac{\partial^2 u_z}{\partial r \partial z} = \rho\frac{\partial^2 u_r}{\partial t^2} \tag{1}$$

$$d_{44}\nabla^2 u_z + d_{33}\frac{\partial^2 u_z}{\partial z^2} + \left(d_{13}+d_{44}\right)\left(\frac{\partial^2 u_r}{\partial r \partial z} + \frac{1}{r}\frac{\partial u_r}{\partial z}\right) = \rho\frac{\partial^2 u_z}{\partial t^2} \tag{2}$$

in which $\nabla^2 = \dfrac{\partial^2}{\partial r^2} + \dfrac{1}{r}\dfrac{\partial}{\partial r}$

In the axisymmetric governing equations, u_r and u_z are the displacement components in r and z directions. d_{ij} and ρ are the components of the elastic modulus and the mass density of the interesting domain, respectively. It is convenient to obtain the following formulations for material constants d_{ij}.

$$d_{11}=d_{33}=\frac{E(1-\upsilon)}{(1+\upsilon)(1-2\upsilon)} \quad d_{12}=d_{13}=\frac{E\upsilon}{(1+\upsilon)(1-2\upsilon)} \quad d_{44}=\frac{E}{2(1+\upsilon)} \tag{3}$$

where E and υ are the Young's modulus and Poisson's ratio of the soil, respectively.

According to the constitutive equations of the elastic solid, the following relationships can be acquired

$$\sigma_{zz}=d_{13}\left(\frac{\partial}{\partial r}+\frac{1}{r}\right)u_r+d_{33}\frac{\partial u_z}{\partial z} \tag{4}$$

$$\tau_{zr}=d_{44}\left(\frac{\partial u_r}{\partial z}+\frac{\partial u_z}{\partial r}\right) \tag{5}$$

where σ_{zz} is the normal stress component in z direction and τ_{zr} is the shear stress in the plane z-r.

For the sake of solving the partial differential equations conveniently, the Hankel transform is considered to convert the partial differential equations into the ordinary differential equations. The Hankel integral transform (Sneddon 1951, 1972) for the function $f(r,z)$ with respect to the variable r is

$$\tilde{f}(k,z)=\int_0^\infty f(r,z)J_m(kr)r\,dr \tag{6}$$

and its inversion is

$$f(r,z)=\int_0^\infty \tilde{f}(k,z)J_m(kr)k\,dk \tag{7}$$

where $\tilde{f}$ (k,z) is the Hankel integral transform for $f(r,z)$; k is the Hankel transform parameter and $J_m(kr)$ stands for the mth order the first kind of Bessel function.

It is assumed that the motion is time-harmonic with circular frequency ω so that u_r and u_z can be denoted as $u_r(r,z,t)=u_r(r,z)e^{i\omega t}$ and $u_z(r,z,t)=u_z(r,z)e^{i\omega t}$. Transforming Eqs. (1) and (2) by applying the Hankel transform with respect to r and the Fourier transformation to t, the following formulations can be obtained

$$(\rho\omega^2-k^2d_{11})\tilde{u}_r+d_{44}\frac{d^2\tilde{u}_r}{dz^2}-(d_{13}+d_{44})k\frac{d\tilde{u}_z}{dz}=0 \tag{8}$$

$$(\rho\omega^2-k^2d_{44})\tilde{u}_z+d_{33}\frac{d^2\tilde{u}_z}{dz^2}+(d_{13}+d_{44})k\frac{d\tilde{u}_r}{dz}=0 \tag{9}$$

where $\tilde{u}_r$ is the result of the first order Hankel transform for u_r and $\tilde{u}_z$ is the result of the zeroth order Hankel transform for u_z.

Eqs. (8) and (9) can be rewritten as follows

$$d_{44}\tilde{u}_r''-(d_{13}+d_{44})k\tilde{u}_z'+(\rho\omega^2-d_{11}k^2)\tilde{u}_r=0 \tag{10}$$

$$d_{33}\tilde{u}_z''+(d_{13}+d_{44})k\tilde{u}_r'+(\rho\omega^2-d_{11}k^2)\tilde{u}_z=0 \tag{11}$$

where $\tilde{u}_z = \dfrac{d^2\tilde{u}_z}{dz^2}$ and $\tilde{u}_r'' = \dfrac{d^2\tilde{u}_r}{dz^2}$.

Substituting $\mathbf{q}=[\tilde{u}_r\ \tilde{u}_z]^T$ into Eqs. (10) and (11) leads to the following second order ordinary differential equations expressed in the matrix form

$$\mathbf{k}_{22}\mathbf{q}''+\left(\mathbf{k}_{21}-\mathbf{k}_{12}\right)\mathbf{q}'-\left(\mathbf{k}_{11}-\rho\omega^2\mathbf{I}\right)\mathbf{q}=\mathbf{0} \tag{12}$$

where $\mathbf{I}$ is a 2×2 unit matrix.

$$\begin{aligned}
\mathbf{k}_{22} &= \begin{bmatrix} d_{44} & 0 \\ 0 & d_{33} \end{bmatrix} \\
\mathbf{k}_{21} &= k\begin{bmatrix} 0 & -d_{44} \\ d_{13} & 0 \end{bmatrix} \\
\mathbf{k}_{12} &= k\begin{bmatrix} 0 & d_{13} \\ -d_{44} & 0 \end{bmatrix} \\
\mathbf{k}_{11} &= k^2\begin{bmatrix} d_{11} & 0 \\ 0 & d_{44} \end{bmatrix}
\end{aligned} \tag{4}$$

Taking the Hankel transform for Eqs. (4) and (5), one can obtain

$$\tilde{\sigma}_{zz} = d_{13}k\tilde{u}_r + d_{33}\frac{d\tilde{u}_z}{dz} \tag{14}$$

$$\tilde{\tau}_{zr} = d_{44}\left(\frac{d\tilde{u}_r}{dz} - k\tilde{u}_z\right) \tag{15}$$

where $\tilde{\tau}_{zr}$ is the result of the first order Hankel transform for τ_{zr} and $\tilde{\sigma}_{zz}$ is the result of the zeroth order Hankel transform for σ_{zz}. From Eqs. (14) and (15), a matrix formulation can be shown as

$$\begin{bmatrix} \tilde{\tau}_{zr} \\ \tilde{\sigma}_{zz} \end{bmatrix} = \begin{bmatrix} d_{44} & 0 \\ 0 & d_{33} \end{bmatrix}\begin{bmatrix} \tilde{u}_r' \\ \tilde{u}_z' \end{bmatrix} + k\begin{bmatrix} 0 & -d_{44} \\ d_{13} & 0 \end{bmatrix}\begin{bmatrix} \tilde{u}_r \\ \tilde{u}_z \end{bmatrix} \tag{16}$$

A dual vector $\mathbf{p}$ is introduced, which can be denoted as

$$\mathbf{p} = -[\tilde{\tau}_{zr}\ \ \tilde{\sigma}_{zz}]^T \tag{17}$$

Substituting the expressions for $\mathbf{k}_{22}$ and $\mathbf{k}_{21}$ into Eq. (16), a formulation can be received

$$\mathbf{p} = -\left(\mathbf{k}_{22}\mathbf{q}'+\mathbf{k}_{21}\mathbf{q}\right) \tag{18}$$

Eqs. (12) and (18) can be written in the state space

$$\mathbf{V}' = \mathbf{H}\mathbf{V} \tag{19}$$

in which $\mathbf{H}=\begin{bmatrix}\mathbf{A} & \mathbf{D}\\ \mathbf{B} & \mathbf{C}\end{bmatrix}$ $\mathbf{V}=\begin{Bmatrix}\mathbf{q}\\ \mathbf{p}\end{Bmatrix}$ and

$$\begin{aligned}\mathbf{A}&=-\mathbf{k}_{22}^{-1}\mathbf{k}_{21}\\ \mathbf{B}&=-\mathbf{k}_{11}+\mathbf{k}_{12}\mathbf{k}_{22}^{-1}\mathbf{k}_{21}+\rho\omega^2\mathbf{I}\\ \mathbf{C}&=\mathbf{k}_{12}\mathbf{k}_{22}^{-1}\\ \mathbf{D}&=-\mathbf{k}_{22}^{-1}\end{aligned} \tag{5}$$

3. Solution procedure

3.1 Boundary conditions

For a multi-layered system the following boundary conditions are considered.

a. At the interface between two adjacent layers, continuity of displacements and stresses is preserved

$$\mathbf{p}\left(z_r^+\right)=\mathbf{p}\left(z_r^-\right),\ \mathbf{q}\left(z_r^+\right)=\mathbf{q}\left(z_r^-\right)\quad\left(r=1,2,3...l+1\right) \tag{21}$$

b. For the multi-layered strata resting on bedrock, it should agree

$$\mathbf{q}_{l+1}=\mathbf{q}\left(z=z_{l+1}\right)=\mathbf{0} \tag{22}$$

c. For a homogeneous isotropic medium underlain by an elastic isotropic half-space, the radiation conditions in the half-space are addressed. It is assumed that the state equation for the semi-infinite space, i.e., the l+1 th layer, is expressed as

$$\bar{\mathbf{V}}'_{l+1}=\mathbf{H}_{l+1}\bar{\mathbf{V}}_{l+1} \tag{23}$$

The eigenvalue equation for $\mathbf{H}_{i+1}$ is

$$\mathbf{H}_{l+1}\mathbf{\Phi}=\mathbf{\Phi}\mathbf{\Lambda} \tag{24}$$

Since $\mathbf{H}_{i+1}$ is the Hamiltonian matrix of the half-space, the eigenvalues can be divided into two groups with the opposite signs and the partitioned forms of $\mathbf{\Lambda}$ and $\mathbf{\Phi}$ are expressed as

$$\mathbf{\Lambda}=\begin{bmatrix}\boldsymbol{\lambda}_i & \\ & -\boldsymbol{\lambda}_i\end{bmatrix}\qquad \mathbf{\Phi}=\begin{bmatrix}\mathbf{\Phi}_{11} & \mathbf{\Phi}_{12}\\ \mathbf{\Phi}_{21} & \mathbf{\Phi}_{22}\end{bmatrix} \tag{25}$$

where the real parts of all elements $\boldsymbol{\lambda}_i$ are positive.

An internal matrix $\mathbf{b}$ is introduced to facilitate the solution process

$$\mathbf{b}=\mathbf{\Phi}^{-1}\bar{\mathbf{V}}_{l+1} \tag{26}$$

Substituting Eqs. (24) and (26) into Eq. (23), a first order ordinary differential equations for $\mathbf{b}$ can be obtained

$$\mathbf{b}' = \mathbf{\Lambda b} \tag{27}$$

The solution for Eq. (27) is

$$\mathbf{b} = \begin{bmatrix} \exp(\boldsymbol{\lambda}_i z) & \\ & \exp(-\boldsymbol{\lambda}_i z) \end{bmatrix} \begin{Bmatrix} \mathbf{c}_1 \\ \mathbf{c}_2 \end{Bmatrix} \tag{28}$$

Substituting Eq. (28) into Eq. (26), the solution expression for Eq. (23) is

$$\bar{\mathbf{V}}_{l+1} = \begin{bmatrix} \mathbf{\Phi}_{11} & \mathbf{\Phi}_{12} \\ \mathbf{\Phi}_{21} & \mathbf{\Phi}_{22} \end{bmatrix} \begin{bmatrix} \exp(\boldsymbol{\lambda} z) & \\ & \exp(-\boldsymbol{\lambda} z) \end{bmatrix} \begin{Bmatrix} \mathbf{c}_1 \\ \mathbf{c}_2 \end{Bmatrix} \tag{29}$$

When $z \to \infty$, the displacement must be zero. In addition, $\boldsymbol{\lambda}$ is a 2×2 diagonal matrix assembled by two positive eigenvalues. So that the integration constant $\mathbf{c}_1$ must be zero. Then one can have

$$\bar{\mathbf{p}}\left(z_{l+1}\right) = \mathbf{\Phi}_{22}\mathbf{\Phi}_{12}^{-1}\bar{\mathbf{q}}\left(z_{l+1}\right) \tag{30}$$

or

$$\bar{\mathbf{p}}\left(z_{l+1}\right) = \bar{\mathbf{R}}_{\infty}\bar{\mathbf{q}}\left(z_{l+1}\right) \qquad \bar{\mathbf{R}}_{\infty} = \mathbf{\Phi}_{22}\mathbf{\Phi}_{12}^{-1} \tag{31}$$

in which $\bar{\mathbf{R}}_{\infty}$ is the stiffness matrix.

3.2 Solutions for the differential matrix equation

Associated derivations and detailed solution procedure are exposed in relevant papers (Lin *et al*. 2013, 2015). In this section, only the concept and key equations necessary for the numerical implementation are presented. Each layer is divided into 2^{N_1} sub-layers of equal thickness and each sub-layer is further divided into 2^{N_2} mini-layers of equal thickness. Then, a typical mini-interval [z_a, z_b] (z_a<z_b) within a layer is taken as an example. Let $\mathbf{q}_a$ and $\mathbf{p}_a$ be the displacement and force vectors at z_a. Similarly, $\mathbf{q}_b$ and $\mathbf{p}_b$ are the displacement and force vectors at z_b. For conservative linear systems, the following relations stand (Zhong *et al*. 1997, Gao *et al*. 2004)

$$\begin{aligned} \mathbf{q}_b &= \mathbf{M}_F^e \mathbf{q}_a - \mathbf{M}_G^e \mathbf{p}_b \\ \mathbf{p}_a &= \mathbf{M}_Q^e \mathbf{q}_a + \mathbf{M}_E^e \mathbf{p}_b \end{aligned} \tag{32}$$

where $\mathbf{M}_F^e$, $\mathbf{M}_G^e$, $\mathbf{M}_Q^e$, $\mathbf{M}_E^e$ are the transfer matrices to be determined.

By the virtue of Eqs. (19) (32) and the technique of Taylor series, one can gain the expressions for the transfer matrices after a series of algebraic manipulation.

After the transfer matrices are determined and with the help of Eq. (32), it is of great convenience to combine any two adjacent intervals [z_a, z_b] and [z_b, z_c] into a new larger interval [z_a, z_c]. The corresponding transfer matrices for the new layer are as follows

$$\mathbf{M}_F^c = \mathbf{M}_F^2 \left(\mathbf{I} + \mathbf{M}_G^1 \mathbf{M}_Q^2\right)^{-1} \mathbf{M}_F^1$$

$$\mathbf{M}_G^c = \mathbf{M}_G^2 + \mathbf{M}_F^2 \left[\left(\mathbf{M}_G^1\right)^{-1} + \mathbf{M}_Q^2\right]^{-1} \mathbf{M}_E^2$$

$$\begin{aligned}\mathbf{M}_Q^c &= \mathbf{M}_Q^1 + \mathbf{M}_E^1\left[\left(\mathbf{M}_Q^2\right)^{-1} + \mathbf{M}_G^1\right]^{-1}\mathbf{M}_F^1 \\ \mathbf{M}_E^c &= \mathbf{M}_E^1\left(\mathbf{I} + \mathbf{M}_Q^2\mathbf{M}_G^1\right)^{-1}\mathbf{M}_E^2\end{aligned} \tag{33}$$

in which the superscript 1 and 2 stand for the transfer matrices of the original intervals [z_a, z_b] and [z_b, z_c] and the superscript c denotes the transfer matrices of the combined larger interval [z_a, z_c]. After determining the transfer matrices for a mini-layer, it's easy to combine two mini-layers together according to the way above.

In a layer each pass of combining two adjacent mini-layers reduces the total mini-layers by a half. When N_2 passes have been operated, the transfer matrices for a sub-layer can be obtained. Combination for two sub-layers is performed directly by taking advantage of Eq. (33). The transfer matrices for a typical layer can be gained after running N_1+N_2 combinations. The whole process is very easy.

Taking a four-layered soil as an example as shown in Fig. 2, the relationship of displacement and stress for each layer is

$$\begin{aligned}\begin{Bmatrix}\mathbf{p}_1 \\ -\mathbf{p}_2^1\end{Bmatrix} &= \begin{bmatrix}\mathbf{K}_{11}^1 & \mathbf{K}_{12}^1 \\ \mathbf{K}_{21}^1 & \mathbf{K}_{22}^1\end{bmatrix}\begin{Bmatrix}\mathbf{q}_1 \\ \mathbf{q}_2^1\end{Bmatrix} \\ \begin{Bmatrix}\mathbf{p}_2^2 \\ -\mathbf{p}_3^2\end{Bmatrix} &= \begin{bmatrix}\mathbf{K}_{11}^2 & \mathbf{K}_{12}^2 \\ \mathbf{K}_{21}^2 & \mathbf{K}_{22}^2\end{bmatrix}\begin{Bmatrix}\mathbf{q}_2^2 \\ \mathbf{q}_3^2\end{Bmatrix} \\ \begin{Bmatrix}\mathbf{p}_3^3 \\ -\mathbf{p}_4^3\end{Bmatrix} &= \begin{bmatrix}\mathbf{K}_{11}^3 & \mathbf{K}_{12}^3 \\ \mathbf{K}_{21}^3 & \mathbf{K}_{22}^3\end{bmatrix}\begin{Bmatrix}\mathbf{q}_3^3 \\ \mathbf{q}_4\end{Bmatrix}\end{aligned} \tag{34}$$

From Eq. (34), the relationship of displacement and force for the global multi-layered soil system is defined as

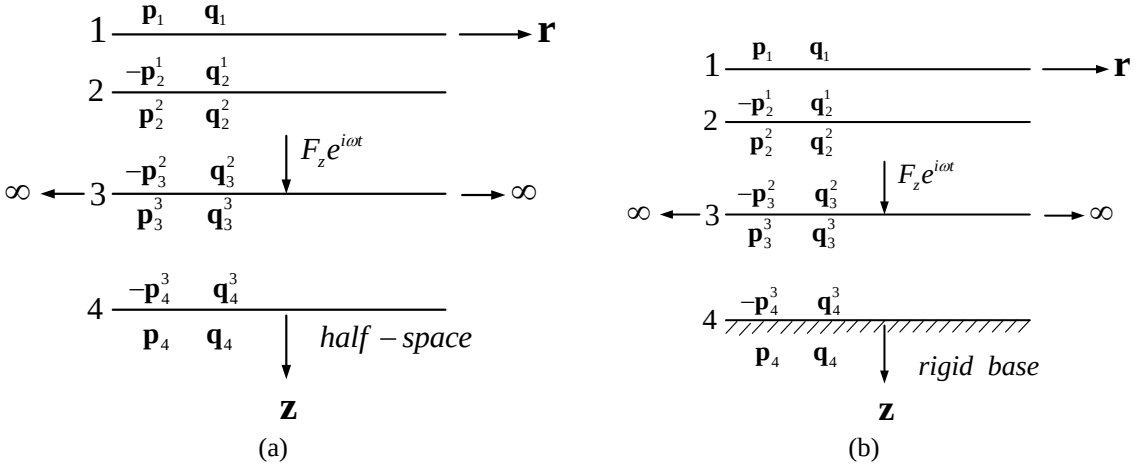

Fig. 2 An example of four-layered soil (a) resting on half-space (b) fixed base

$$\begin{Bmatrix}\mathbf{P}_1\\ \mathbf{P}_2\\ \mathbf{P}_3\\ \mathbf{P}_4\end{Bmatrix}=\begin{bmatrix}\mathbf{K}_{11}^1 & \mathbf{K}_{12}^1 & & \\ \mathbf{K}_{21}^1 & \mathbf{K}_{22}^1+\mathbf{K}_{11}^2 & \mathbf{K}_{12}^2 & \\ & \mathbf{K}_{21}^2 & \mathbf{K}_{22}^2+\mathbf{K}_{11}^3 & \mathbf{K}_{12}^3\\ & & \mathbf{K}_{21}^3 & \mathbf{K}_{22}^3+\mathbf{K}_{\infty}\end{bmatrix}\begin{Bmatrix}\mathbf{U}_1\\ \mathbf{U}_2\\ \mathbf{U}_3\\ \mathbf{U}_4\end{Bmatrix}$$

$$\mathbf{P}=\mathbf{K}\mathbf{U} \tag{35}$$

where $\mathbf{P}=\begin{bmatrix}\mathbf{P}_1 & \mathbf{P}_2 & \mathbf{P}_3 & \mathbf{P}_4\end{bmatrix}^T$ $\mathbf{U}=\begin{bmatrix}\mathbf{U}_1 & \mathbf{U}_2 & \mathbf{U}_3 & \mathbf{U}_4\end{bmatrix}^T$

$\mathbf{P}_1=\mathbf{p}_1$ $\mathbf{P}_2=-\mathbf{p}_2^1+\mathbf{p}_2^2$ $\mathbf{P}_3=-\mathbf{p}_3^2+\mathbf{p}_3^3$ $\mathbf{P}_4=-\mathbf{p}^3{}_4+\mathbf{p}$

$\mathbf{U}_1=\mathbf{q}_1$ $\mathbf{U}_2=\mathbf{q}_2^1=\mathbf{q}_2^2$ $\mathbf{U}_3=\mathbf{q}_3^2=\mathbf{q}_3^3$ $\mathbf{U}_4=\mathbf{q}_4^3=\mathbf{q}_4$

$\mathbf{p}_4=\mathbf{K}_{\infty}\mathbf{q}_4$

In Eq. (35), **P** stand for the external force vectors and **U** are unknown displacements. From Eq. (35), **K** are the stiffness matrix composed by the transfer matrices for the whole stratified system in the Hankel transform domain. For a multi-layered half-space, $\mathbf{K}_\infty$ are the stiffness matrix for the half-space layer, which is the matrix $\bar{\mathbf{R}}_\infty$ in Eq. (31). For the case of layered soil resting on rigid base, $\mathbf{K}_\infty$ must be equal to zero.

4. Transfer to physical space domain

The case of a vertically concentrated dynamic force of the unit amplitude acting on the symmetric axis of the cylindrical coordinate system is addressed. At first, in order to solve the problem conveniently it is advantageous to assume that the force is uniformly distributed in a circular disk with the radius R ($R\to 0$) R and the amplitude of the uniform force is $p_{z0}=\dfrac{1}{\pi R^2}$. Applying the Hankel integral transform to p_{z0}, one can obtain

$$\begin{aligned}\tilde{p}_z(k)&=\int_0^\infty p_z(r)J_0(kr)rdr=\int_0^R p_z(r)J_0(kr)rdr\\ &=\int_0^R p_{z0}J_0(kr)rdr=\frac{1}{k}Rp_{z0}J_1(kR)\end{aligned} \tag{36}$$

where $\tilde{p}_z(k)$ is the result of the zeroth order Hankel transform for p_{z0}. The zeroth order Hankel transform for a point load is

$$\lim_{R\to 0}\tilde{p}_z(k)=\lim_{R\to 0}\frac{1}{k}Rp_{z0}J_1(kR)=\frac{1}{2\pi} \tag{37}$$

Substituting Eq. (37) into Eq. (35), the displacements for each layer in the multi-layered soil can be obtained.

$$u_r(r,z,\omega)=\int_0^\infty \tilde{u}_r(k,z,\omega)J_1(kr)kdk \tag{38}$$

$$u_z(r,z,\omega)=\int_0^\infty \tilde{u}_z(k,z,\omega)J_0(kr)kdk \tag{39}$$

$$\tau_{zr}(r,z,\omega)=\int_0^\infty \tilde{\tau}_{zr}(k,z,\omega)J_1(kr)kdk \tag{40}$$

$$\sigma_{zz}(r,z,\omega)=\int_0^\infty \tilde{\sigma}_{zz}(k,z,\omega)J_0(kr)kdk \tag{41}$$

The displacements and stresses in physical space domain could be obtained by taking the numerical inversion of Hankel transforms. As indicated in the previous equations, the displacement and stress components are expressed in terms of one-dimensional semi-infinite integrals. As the integrations generally cannot be carried out in exact closed forms, a numerical quadrature technique usually has to be adopted in such evaluations.

5. Numerical examples

In this section, several examples are illustrated to evaluate the accuracy and the efficiency of the current solutions. They are followed by a series of parametric study to explore the influence of stratified characters, the frequency of excitation and the positions of loading on the dynamic response of the homogeneous medium. When one factor is discussed, the other factors would remain constant. It needs to point out that all numerical results presented here are dimensionless, with a non-dimensional frequency defined as $\omega_0 = L\omega\sqrt{\rho/G}$ and the normalized vertical displacement $\bar{u}_z = Gu_z/(F_zL)$, where L is the unit of characterized length.

5.1 Verification

The following three examples are employed to compare the present solutions with the existing numerical solutions in order to elucidate the feasibility of the proposed method. The first two examples (Ai *et al*. 2002) are about an isotropic half-space and an elastic three-layered media with rigid base, respectively. Both examples are under a static concentrated load. The third example (Khojasteh *et al*. 2008) involves a homogeneous semi-infinite domain subjected to a time-harmonic point load.

5.1.1 Homogeneous elastic half-space

The solutions for a vertical load F_z concentrating at the origin of the coordinate system and acting in the interior of the media for a homogenous elastic half-space are the classical Boussinesq solutions and Mindlin's solutions, respectively.

In this example, a static point load is applied on the surface of an elastic half-space. In order to satisfy the static case, the excitation frequency is chosen ω_0=0.

Fig. 3 illustrates the variations of the vertical displacement due to the vertically concentrated load acting on the surface of the homogeneous elastic half-space with the depth z/r off the axis of loading (r=1) and presents a comparison of the solution form the proposed approach with the Boussinesq solution. Wonderful agreement between the two solutions demonstrates the effectiveness of the proposed approach to deal with the homogeneous elastic half-space.

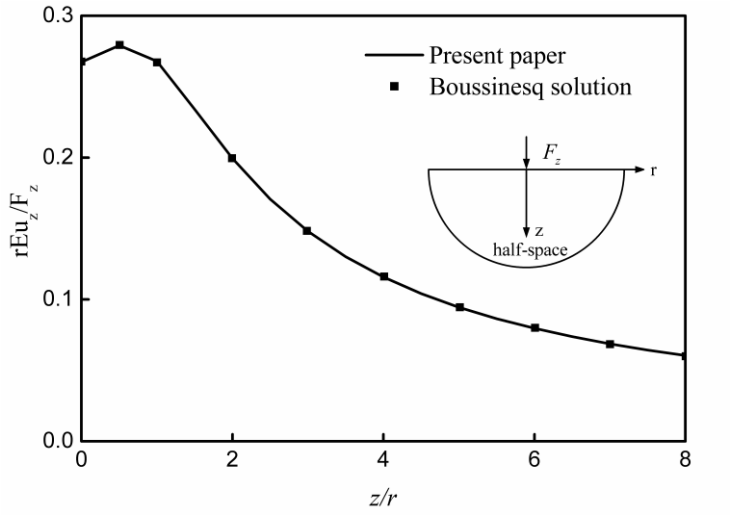

Fig. 3 Variations of the dimensionless vertical displacement due to the vertical point load on the surface of the elastic half-space with the depth z/r off the axis of loading (r=1)

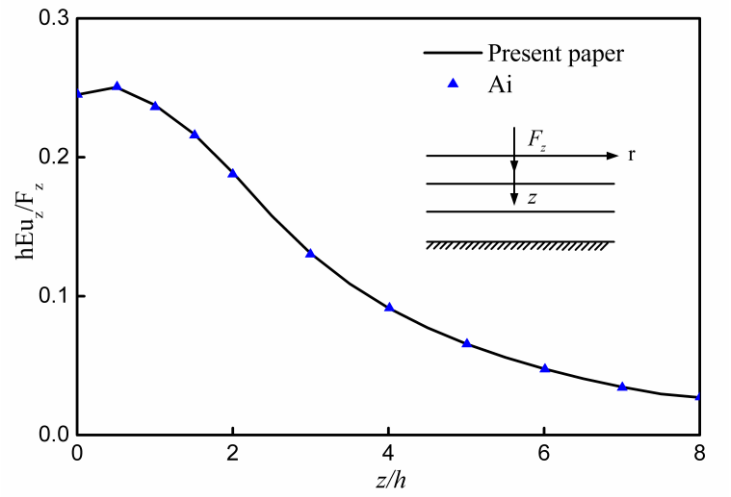

Fig. 4 Variations of the normalized displacement due to the vertical point load F_z in the interior of the three-layered soil with the depth z/r off the axis of loading (r/h=1) for case1

5.1.2 Three-layered soil with rigid base

From the paper (Ai *et al*. 2002), there is an example of the displacement field in a three-layered elastic material with the bottom plane fixed subjected to a vertical point load. The case of the vertical point load acting on the point (0,0,h) in the elastic layers attracts our attention. The material parameters for all cases are listed in Table 3 (Ai *et al*. 2002).

Figs. 4-6 show the normalized vertical displacements for three different cases. From those figures, it is clearly observed that the numerical results from the proposed method are nearly the same as those from Ai *et al*. (2002), which describes that the proposed method can solve the problem of the multi-layered soil with the bottom fixed effectively.

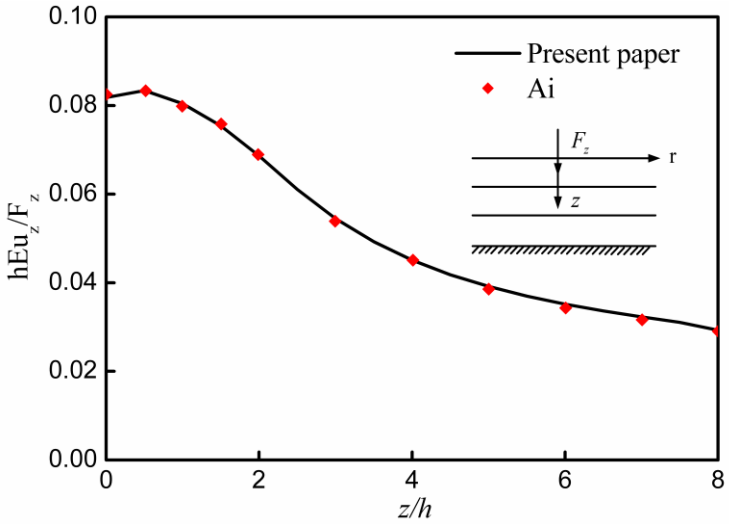

Fig. 5 Variations of the normalized displacement due to the vertical point load F_z in the interior of the three-layered soil with the depth z/h off the axis of loading (r/h=1) for case2

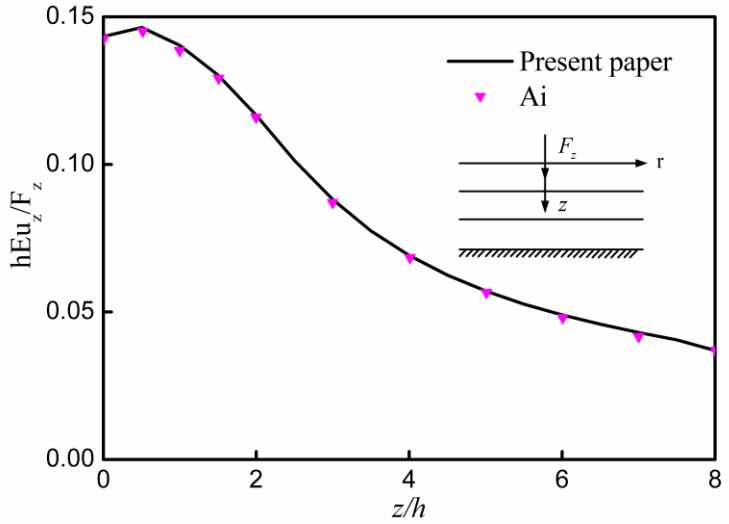

Fig. 6 Variations of the normalized vertical displacement due to the vertical point load F_z in the interior of the three-layered soil with the depth z/h off the axis of loading (r/h=1) for case3

5.1.3 Half-space under dynamic load

In order to provide a comparison of the results for a dynamic case, the solution (Khojasteh *et al*. 2008) for the displacement in z-direction along the r axis induced by a time-harmonic point load of unit intensity with a dimensionless frequency ω_0=0.5 is used as a benchmark. The elastic parameters of the medium are G=10 Gpa and υ=0.25. As indicated in Fig. 7, there is an excellent agreement between the solutions of this paper and the solutions obtained (Khojasteh *et al*. 2008) for both real and imaginary parts. Consequently, the effectiveness of the method in this part has been confirmed.

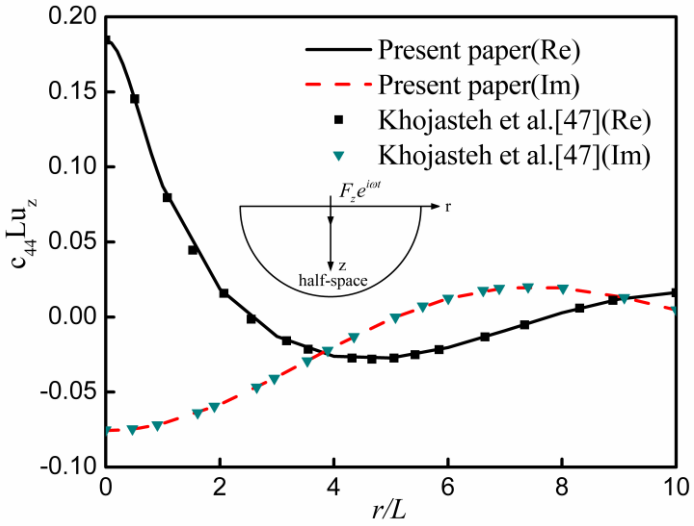

Fig. 7 Variations of the non-dimensional vertical displacements due to a vertical point load along free surface

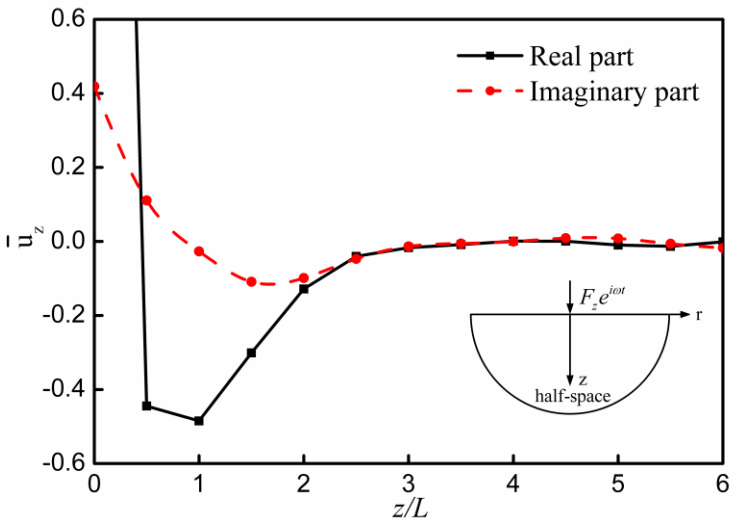

Fig. 8 Variations of the vertical displacements under the vertical point load acting on the surface of the homogeneous elastic half-space with the depth on the axis of loading

5.2 Influence of the loading location

In order to present the effect of the loading position, a degenerated example of a homogeneous isotropic half-plane is carried out. A time-harmonic point load is applied on and within the soil system. The mass density of the medium is ρ=3.0×10^3 kg/m^3; the Poisson's rations is υ=0.25 and the normalized frequency is ω_0=3.0. Three cases of different loading depth s=0, 2L, 5L are discussed in details. In this part, it is worth mentioning that the vertical displacements off the axis of loading are along the axis r/L=1 and the variable r stands for the distance off the loading

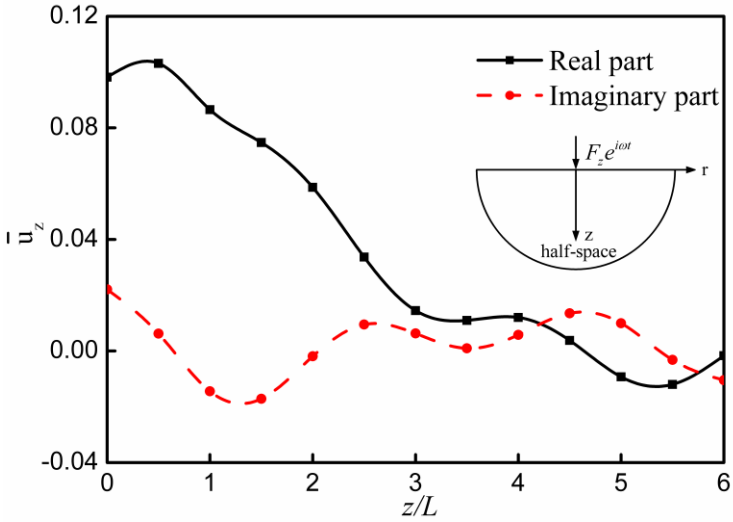

Fig. 9 Variations of the vertical displacements under the vertical point load acting on the surface of the homogeneous elastic half-space with the depth off the axis of loading

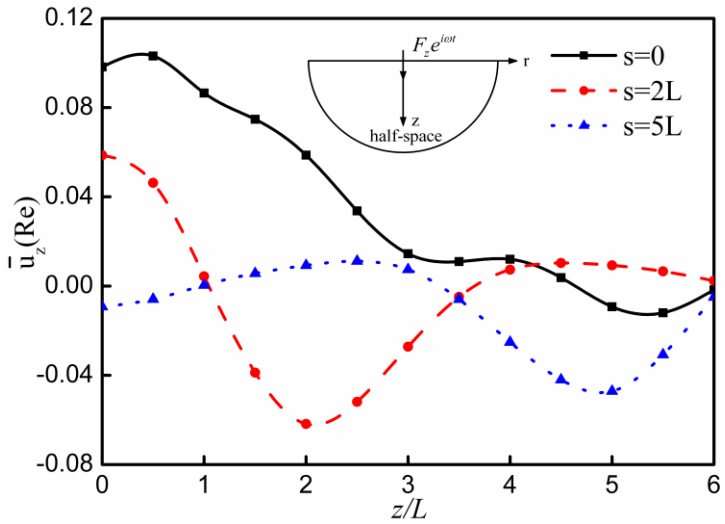

Fig. 10 Comparisons of the real parts of the vertical displacements off the axis of loading due to a point load

location. The calculating results of the vertical displacement against the normalized depth under the action of a point load acting on the surface of an isotropic half-space are plotted in Figs. 8-9, respectively. Figs. 10-11 describe the variations of the vertical displacement with the depth off the axis of loading caused by the vertically concentrated loading acting on the surface and in the interior of the semi-infinite domain.

As indicated in Fig. 8, the real part of the maximum displacement is noted at the depth where the load is applied. However, both the real and imaginary parts of the displacement in vertical

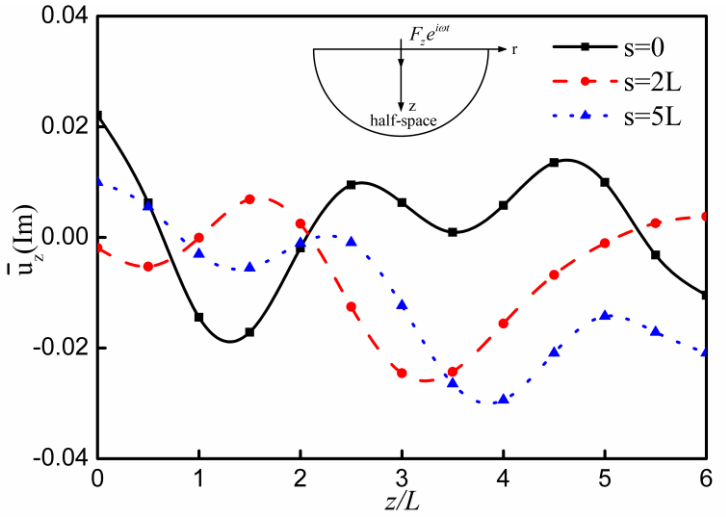

Fig. 11 Comparisons of the imaginary parts of the vertical displacements off the axis of loading due to a point load

direction in Fig. 9 don't copy this phenomenon. It is concluded that one of the most important features of point load solutions is the presence of the singularities at the loading position. On the contrary, the distribution curves of the displacement off the loading location are smoother. As shown in Figs. 10-11, the real parts of the vertical vibration amplitude on the surface decrease with the point load moving down. Meanwhile, the curves of real parts give rise to a kink at the horizontal stratum where the load is applied. Moreover, with the increase of depth, the real parts of the vibration amplitude decrease. The real parts tend to zero when the depth is large enough. As for the loading depth, the imaginary parts exhibit complicated pattern.

5.3 Influence of material characters

Additional examples are considered to reveal the influence of elastic material characters on the vertical deformations. In order to simplify the analysis, a model of an isotropic, linearly elastic layer bonded to the surface of a half-space of a different isotropic material is chosen. It is meaningful to point out that in order to avoid the singularity, point load solutions are along the axis r/L=1, in which the variable r represents the distance off the loading location. Meanwhile, the parameter G stands for the shear modulus of the top stratum in the non-dimensional frequency and vertical settlement.

5.3.1 Influence of shear modulus

The first example is about the influence of shear modulus on the magnitude of the vertical solutions. The remaining elastic parameters are υ_1=υ_2=0.25 and ω_0=3.0. The boundary between the top layer and the substrate is set at h=2L. Figs. 12-15 depict the real and imaginary parts of the normalized vertical displacements at different depth induced by a time-harmonic point load acting on and within the solid media, respectively. In Figs. 12-13, the phenomenon that the stiffness of the lower layer has a significant effect on displacements attracts our attention. Both the real and imaginary parts of the case E_1:E_2=1:5 are prodigiously changeable. In addition, it is apparent that

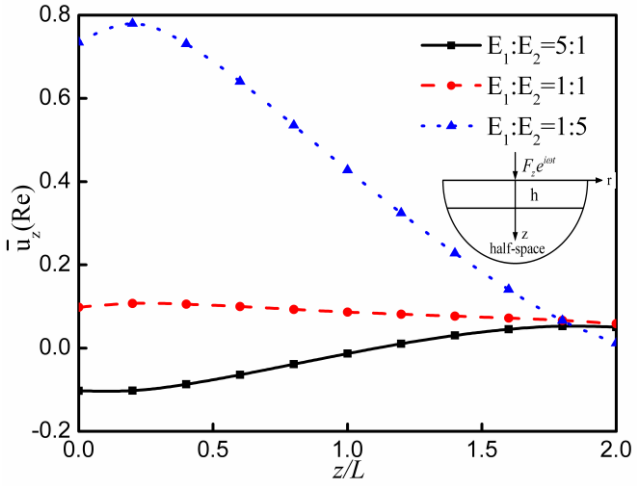

Fig. 12 Results of the real parts of the vertical displacements against normalized depth caused by the surface point load

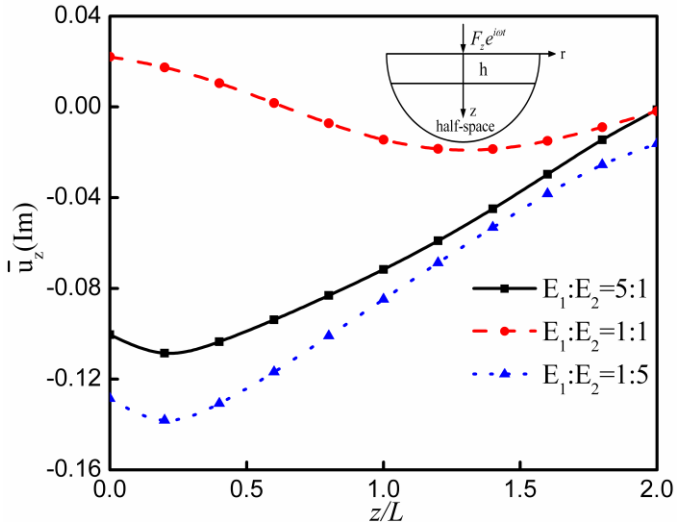

Fig. 13 Results of the imaginary parts of the vertical displacements against normalized depth caused by the surface point load

with the depth increase, the solutions in all three cases tend to zero. However, the displacement field from Figs. 14-15 don't show the same basic characteristics as described earlier. The solutions are markedly more influenced by the upper layer under the situation of the load application on the interface. Since the load is applied in the interior, the negative maxima of the real and imaginary parts occur at the loading level in the case of E_1:E_2=5:1.

5.3.2 Influence of poisson's ratio

Two sets of examples are illustrated to consider the effect of Poisson's ratio. Let E_1:E_2=1:4, ρ=3.0×10^3 kg/m^3 and the dimensionless frequency ω_0=3.0. At first, three cases of υ_1=υ_2=0.1,

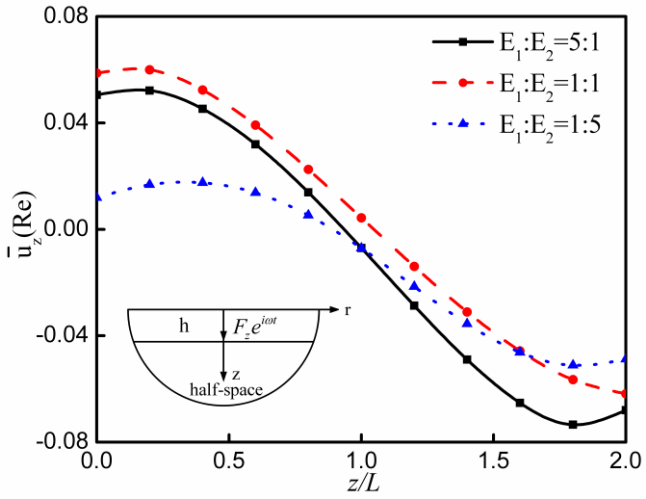

Fig. 14 Results of the real parts of the vertical displacements against normalized depth caused by the interface point load

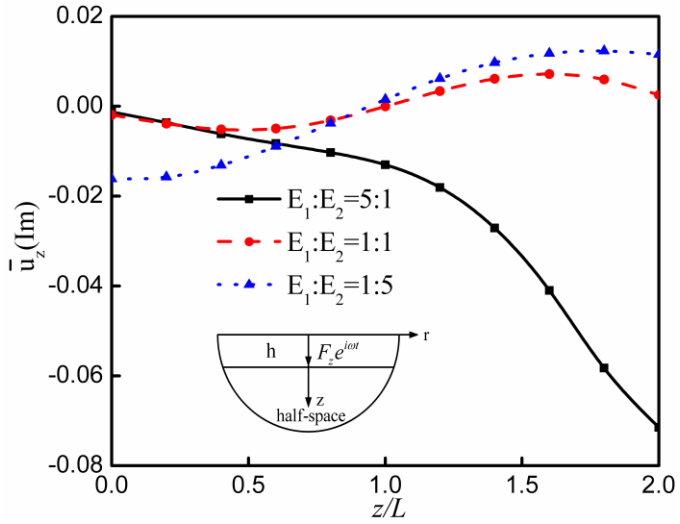

Fig. 15 Results of the imaginary parts of the vertical displacements against normalized depth caused by the interface point load

υ_1=υ_2=0.25 and υ_1=υ_2=0.4 are performed for comparisons. The variations of the normalized vertical displacement with the depth off the axis of loading under the vertically concentrated force applied on the surface and on the interface of the two-layered soil are portrayed in Figs. 16-19. Following this way, the comparisons of υ_1=0.1, υ_1=0.25 and υ_1=0.4 are considered. The Poisson's ratios of the half-space in three cases are equal to 0.25. Figs. 20-23 illustrate the variations of the real and imaginary parts of the normalized vertical settlement in terms of normalized depth z/L with the concentrated time-harmonic loading applied on the surface and in the interior of the research domain. From Figs. 16-17, it is obvious that there are dramatic changes in both the real and imaginary parts of the normalized vertical displacement in case 2 when the external load is

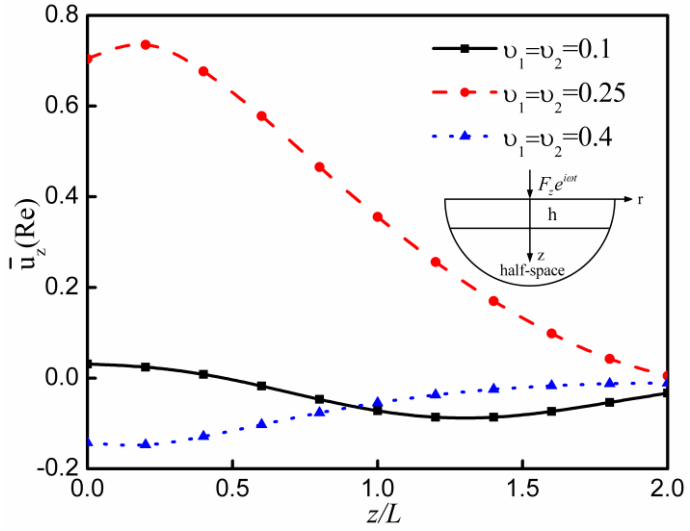

Fig. 16 Real parts of the normalized vertical displacements due to the concentrated force on the surface

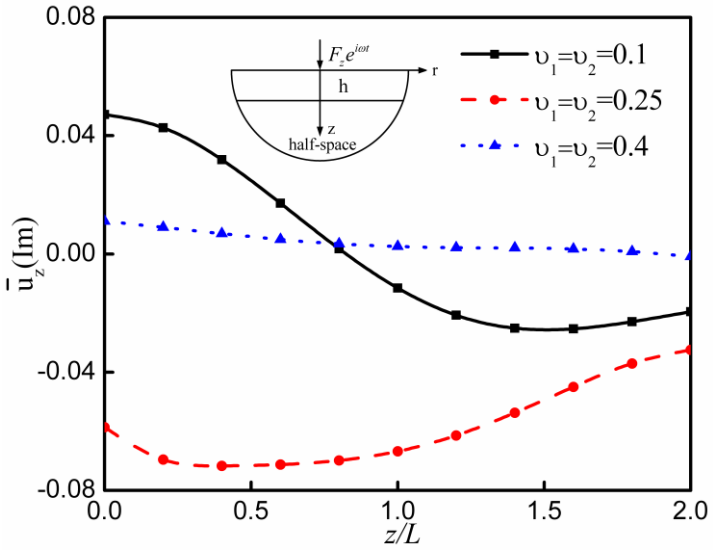

Fig. 17 Imaginary parts of the normalized vertical displacements due to the concentrated force on the surface

applied on the surface of the interesting domain. As illustrated in Figs. 18-19, the difference between the maximum and minimum values of the displacement curve is great in case 1, in which the load is acting on the interface of the medium. Similarly, both the real and imaginary parts of case 1 intensely vary along the normalized depth when the point load is employed either on the surface or in the interior of the stratified system in Figs. 20-23. A conclusion may be drawn that the Poisson's ratio of the top layer causes significant influence on the displacement field. Thus, medium's stratified parameter and the loading depth have a great effect on the vertical displacement, which should not be neglected in practical engineering.

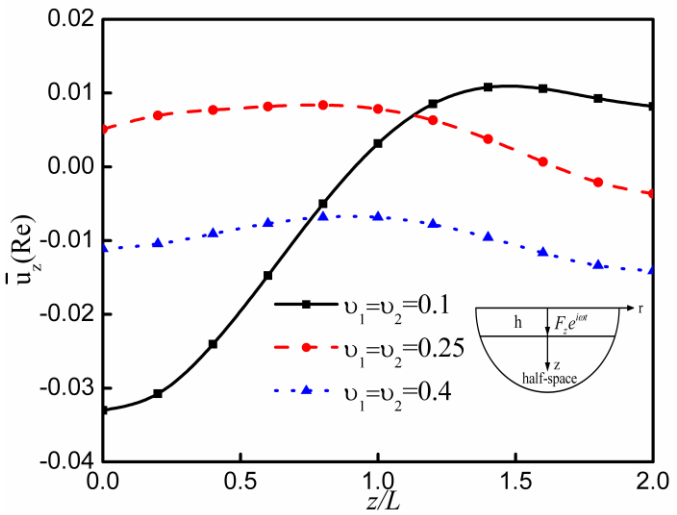

Fig. 18 Real parts of the normalized vertical displacements due to the concentrated force on the interface

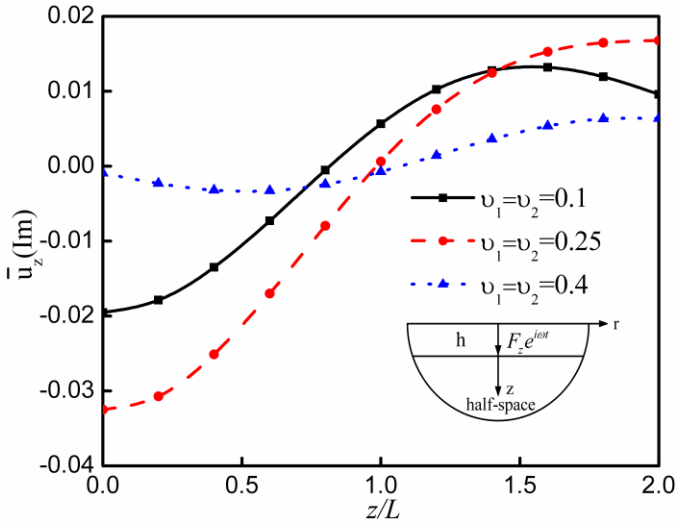

Fig. 19 Imaginary parts of the normalized vertical displacements due to the concentrated force on the interface

5.4 Effect of thicknesses of the layer

For most of the geotechnical situations, layered formations with different material properties are usually encountered in practical engineering. Herein the four layered geo-materials are selected as an example to demonstrate the influence of thicknesses of the medium strata on the elastic field. The elastic parameters are listed E_1:E_2:E_3:E_4=1.0:1.5:2:2.5, ρ_i=3000 kg/m^3, υ_i=0.25 (i=1,2,3 and 4) and the non-dimensional frequency ω_0=3.0. Three cases of different thicknesses are illustrated for discussion (1) h_1:h_2:h_3:L=8:1:1:1, (2) h_1:h_2:h_3:L=1:8:1:1 and (3) h_1:h_2:h_3:L=1:1:8:1. In the

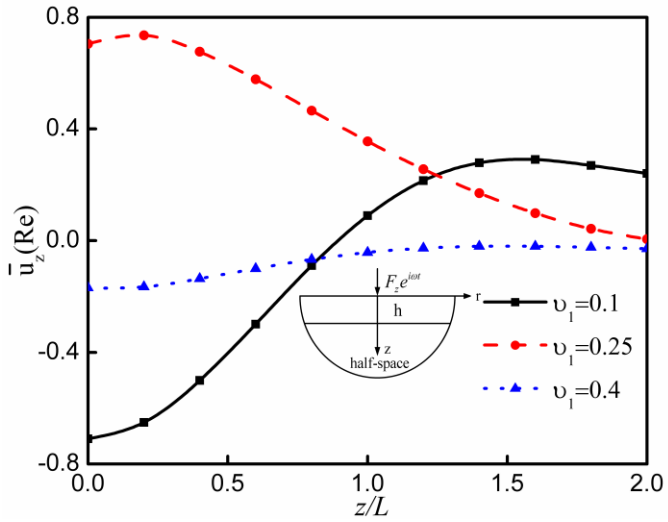

Fig. 20 Influence of Poisson's ratio on the real parts of the normalized vertical displacements subjected to the concentrated load acting on the outer boundary

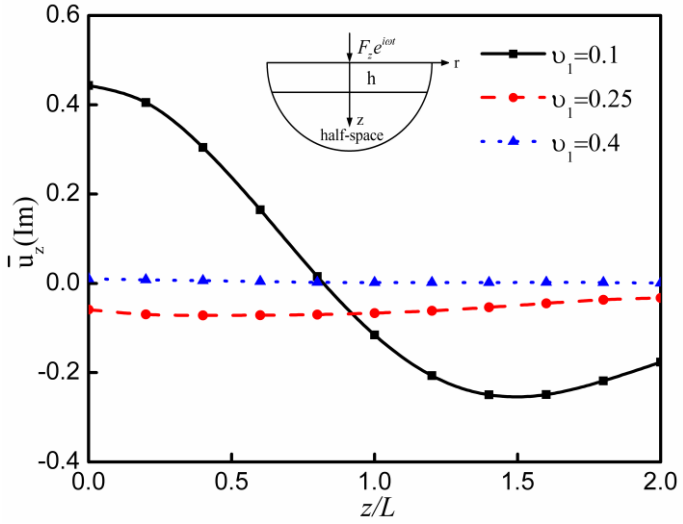

Fig. 21 Influence of Poisson's ratio on the imaginary parts of the normalized vertical displacements subjected to the concentrated load acting on the outer boundary

following pictures, the normalized vertical deformations due to a point load concentrated on the surface of the four layered medium or at the interior point $(0,0,h_1+h_2+h_3)$ are along the axis r/L=1. The variable r means the distance off the loading position. In the non-dimensional frequency and vertical displacement, the parameter G indicates the shear modulus of the first layer. Results of the vertical displacement against normalized depth under the action of concentrated forces applied on the surface and in the interior of the four-layered homogeneous isotropic media are plotted in Figs. 24-27, respectively. As indicated in all figures, the case of h_1:h_2:h_3:L=8:1:1:1 which has the thickest top layer is much more different from other cases. Moreover, the magnitudes of the

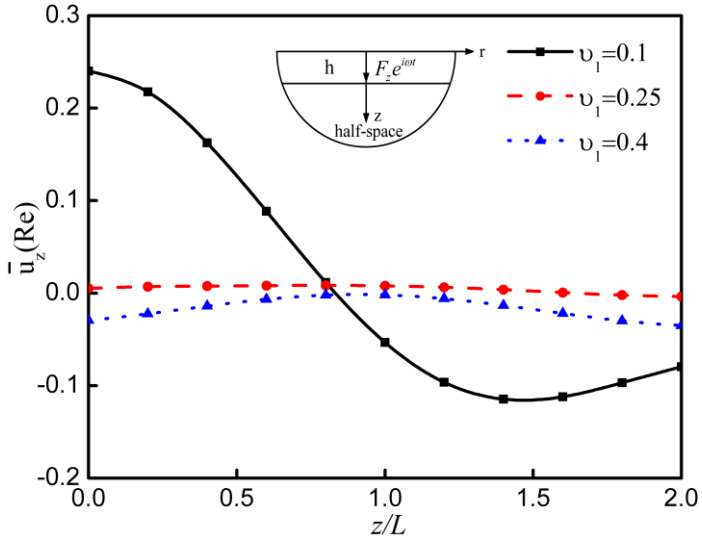

Fig. 22 Influence of Poisson's ratio on the real parts of the normalized vertical displacements subjected to the concentrated load acting on the inner interface

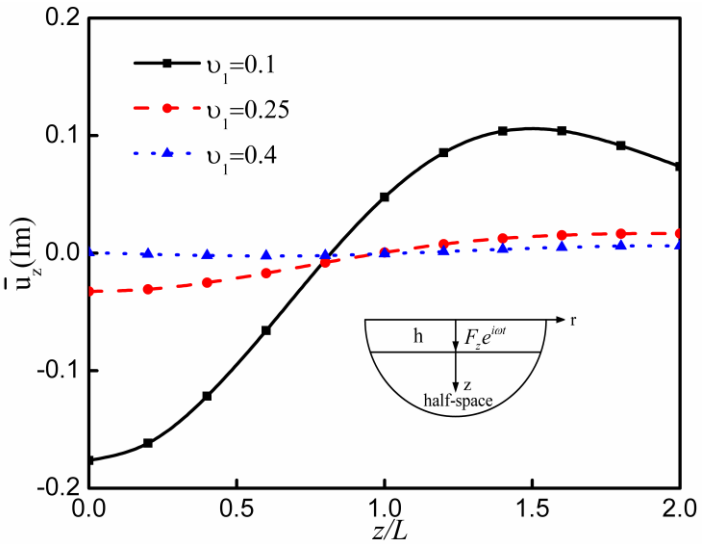

Fig. 23 Influence of Poisson's ratio on the imaginary parts of the normalized vertical displacements subjected to the concentrated load acting on the inner interface

vertical displacements in this case violently oscillate regardless of the point loading prescribed either at the external surface or within the multi-layered materials. At the same time, the real parts of vertical results on the surface in case 1 are larger than that of case 2 and case 3. The curvilinear shapes of the vertical displacement in case 2 and case 3 are analogous. All the appearances demonstrate that the variations of the normalized vertical displacements are more sensitive to the thickness of the top layer.

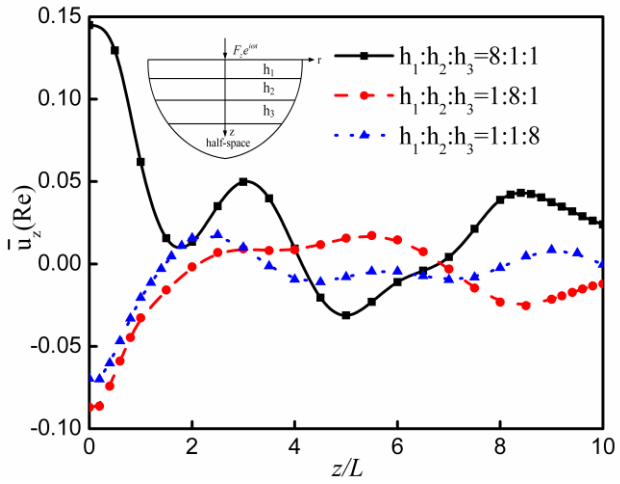

Fig. 24 Effect of different thicknesses on the real parts of the normalized vertical displacements with the point load acting on the surface of the multi-layered media

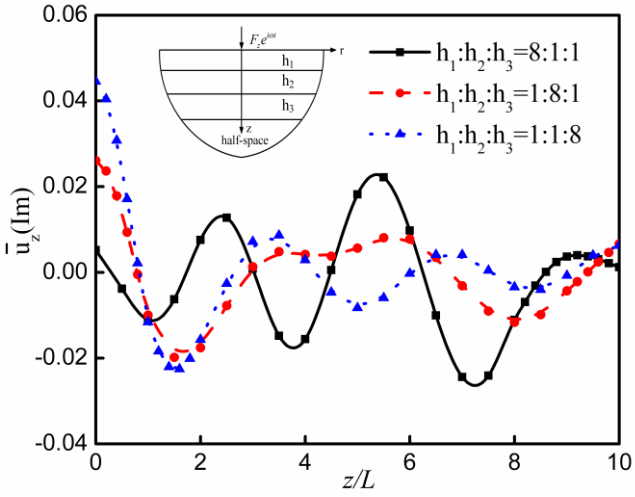

Fig. 25 Effect of different thicknesses on the imaginary parts of the normalized vertical displacements with the point load acting on the surface of the multi-layered media

5.5 Influence of the excitation frequency

It has been well recognized that the occurrence of time-varying displacements under external forces is quite common in engineering practice. Excitation frequency is a basic and key factor of time-harmonic external loading. So it is essential to explore the influence of the excitation frequency on the distribution of normalized vertical displacements in the multi-layered medium. An example of four layered soil as the previous section is chosen to investigate the influence of the excitation frequency. The corresponding relationships of the elastic material parameters are as follows: E_1:E_2:E_3:E_4=1.5:2:3.5:5, ρ_i=3×10^3 kg/m^3, υ_i=0.25 (i=1,2,3,4) and h_1:h_2:h_3:L=1:2:3:1. There are four cases of frequency range discussed, which are ω_0=0.5,3.0,5.0,10.0, respectively. To

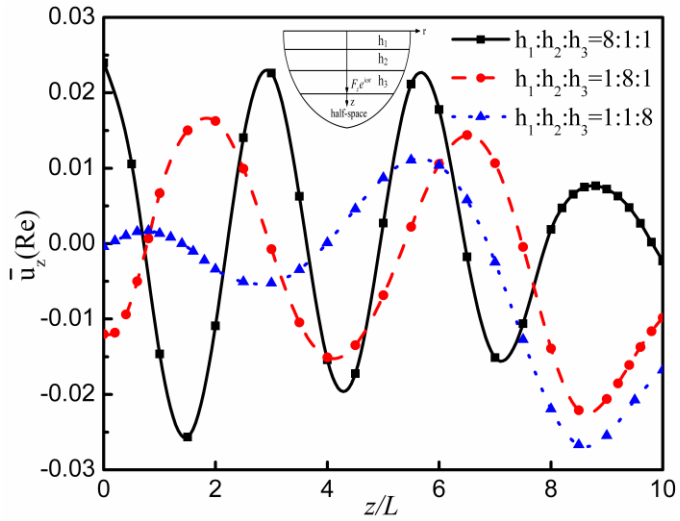

Fig. 26 Influence of different thicknesses on the real parts of the normalized vertical displacements under the point load applied in the interior of the system

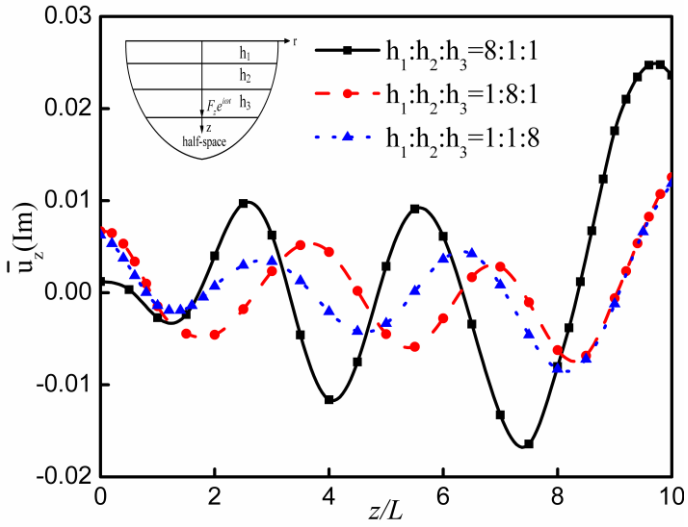

Fig. 27 Influence of different thicknesses on the imaginary parts of the normalized vertical displacements under the point load applied in the interior of the system

maintain consistency with the previous sections, the vertical displacements are also along the axis r/L=1 and the material parameter G of the non-dimensional frequency and vertical displacement denotes the shear modulus of the top layer. Figs. 28-31 plot the real and imaginary parts of normalized displacements in vertical direction induced by the external loading concentrated at a point acting with different frequencies. From the displays, one may observe that the influence of the excitation frequency of the time-harmonic loading is obviously evident on vertical displacement solutions. As frequency increases, both real and imaginary parts show more oscillatory variation with the depth. At low frequencies, both real and imaginary parts decays

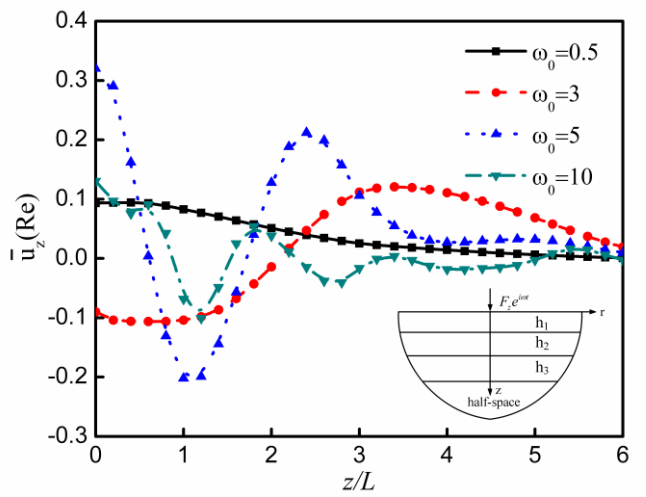

Fig. 28 Variations of the real parts of the vertical displacements with respect to *z/L* under a concentrated load applied on the surface of the exterior boundary

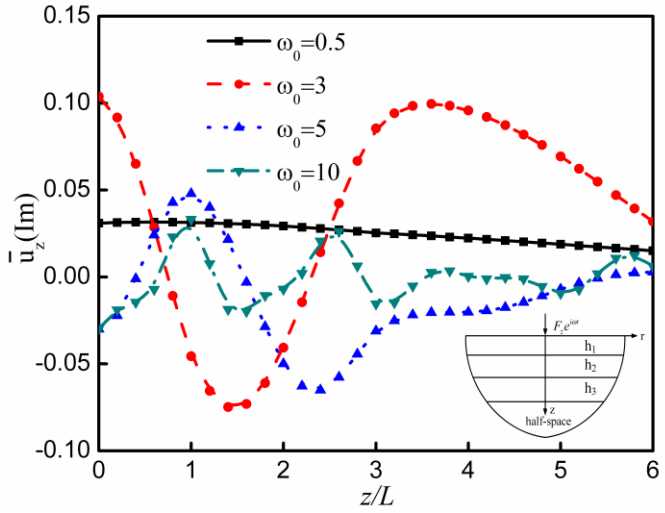

Fig. 29 Variations of the imaginary parts of the vertical displacements with respect to *z/L* under a concentrated load applied on the surface of the exterior boundary

smoothly along with depth under a surface loading. What's more, it is also shown that unlike previous observations, the unified variation of the amplitude of vertical displacements with increasing frequencies is not obvious. Variations of both the real and imaginary parts of the non-dimensional vertical displacements are more complicated when frequencies are increasing. Either the real or the imaginary parts of the vertical settlements tend to zero with the increasing depth when the load is acting on the surface of the research domain in Figs. 28-29. However, form Figs. 30-31 the real and imaginary parts of the displacements induced by concentrated forces applied within the stratified soil don't arise this phenomenon. The solutions delineate that variations of the displacement field are decisively affected by the frequency of excitation.

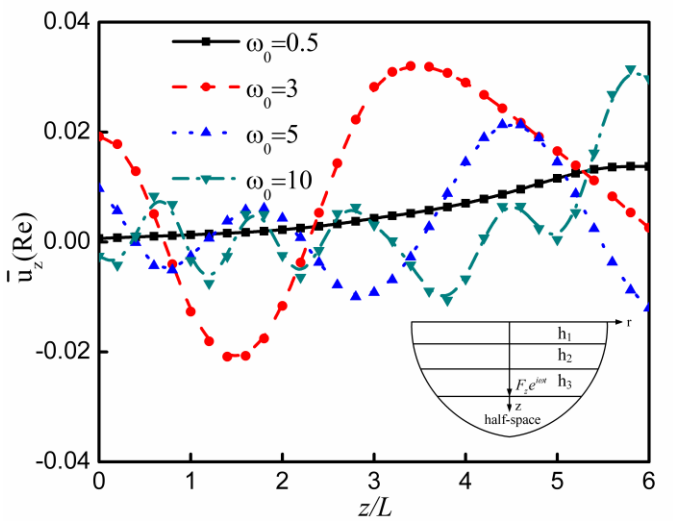

Fig. 30 Variations of the real parts of the vertical displacements with respect to *z*/*L* due to a point load acting on the interior interface

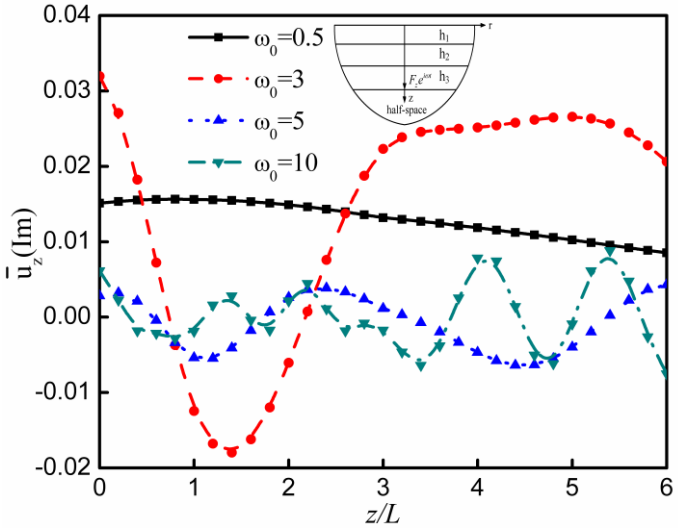

Fig. 31 Variations of the imaginary parts of the vertical displacements with respect to *z*/*L* due to a point load acting on the interior interface

6. Conclusions

In this paper, solutions for the axisymmetric elastodynamic response in a continuously homogeneous isotropic multilayered media are presented by employing the proposed method. The precise integration algorithm and mixed variable formulation ensure the accuracy and effectiveness of the proposed approach. According to the Hankel integral transform and mixed variable formulation, the partial differential equations are conveniently converted into ordinary differential equations. The point load solutions are extremely precise for the precise integration

method is a highly accurate method to solve sets of first-order ordinary differential equations. To obtain the space domain displacements, it is essential to take the numerical inversion of the Hankel transform. All calculation is based on the standard matrix algebra method. Computational effort can be reduced to a great extent for the size of the transfer matrices is not larger than 2×2. Comparing with the analytical solutions reveals that the field of vertical displacements from the proposed process is precise. There is no problem for this method to simulate the multi-layered stratum with all kinds of boundary conditions. From the figures above, it is obvious that one of the most important features of point load solutions is the presence of the singularities at the loading position. But the curves of the dimensionless vertical settlements off the axis of the external loading tend to be smooth. The loading depth has a remarkable influence on the magnitude and distribution of the displacements. When the load moves down, the displacement amplitude at the surface decreases. Moreover, the real parts of the displacements give rise to a kink at the depth of the applied load. As to the stratified character, influences of the shear modulus and the Poisson's ratio on the normalized displacements vary as the loading position. In addition, the frequency of excitation has an obvious effect on the vertical displacement as well. With the frequency increasing, the real and imaginary parts of the point load solutions become increasingly oscillatory. Solutions presented in this paper can be of great value in developing solutions for analytical examination of elastic problems and incorporated into numerical schemes such as boundary element methods for numerical analysis of elastostatic and elastodynamic problems.

Acknowledgements

This research was supported by Grant 51409038 from the National Natural Science Foundation of China, Grant No. 51421064 from Science Fund for Creative Research Groups of the National Natural Science Foundation of China, Grants 2013M530919 and 2014T70251 form China Postdoctoral Science Foundation, Grant GZ1406 from the Open Foundation of State Key Laboratory of Structural Analysis for Industrial Equipment, Grant 51138001 from the State Key Program of National Natural Science of China, and Grant 1202 from Open Foundation of State Key Laboratory of Ocean Engineering, Grant L2013016 from Liaoning Province Department of Education Research Project, and Grant DUT15RC(4)23 from the fundamental research funds for the central universities for which the authors are grateful.

References

Ai, Z.Y., Yue, Z.Q., Tham, L.G. and Yang M. (2002), "Extended Sneddon and Muki solutions for multilayered elastic materials", *Int. J. Eng. Sci.*, **40**(13), 1453-1483.

Apsel, R.J. and Luco, J.E. (1983), "On the Green's functions for a layered half-space. Part II", *Bull. Seismol. Soc. Am.*, **73**(4), 931-951

Benitez, F.G. and Rosakis, A.J. (1987), "Three-dimensional elastostatics of a layer and a layered medium", *J. Elast.*, **18**(1), 3-50.

Birk, C. and Behnke, R. (2012), "A modified scaled boundary finite element method for three-dimensional dynamic soil-structure interaction in layered soil", *Int. J. Numer. Meth. Eng.*, **89**(3), 371-402.

Boussinesq, J. (1885), *Application des Potentials à Létude de Léquilibre et du Mouvement des Solides élastiques*, Gauthier-Villars, Paris, Paris.

Bufler, H. (1971), "Theory of elasticity of a multilayered medium", *J. Elast.*, **1**(2), 125-143.

Burmister, D.M. (1945), "The general theory of stresses and displacements in layered systems, I", *J. Appl. Phys.*, **16**(2), 89-94.
Burmister, D.M. (1945), "The general theory of stresses and displacements in layered soil systems. II", *J. Appl. Phys.*, **16**, 126-127.
Burmister, D.M. (1945), "The general theory of stresses and displacements in layered soil systems. III", *J. Appl. Phys.*, **16**(5), 296-302.
Burmister, D.M. (1956), "The stresses and displacement characteristics of a two layer rigid base soil system: Influence diagrams and practical applications", *Highw. Res. Board Pr.*, **35**, 773-814.
Chan, K.S, Karasudhi, P. and Lee, S.L. (1974), "Force at a point in the interior of a layered elastic half space", *Int. J. Solid. Struct.*, **10**(11), 1179-1199.
Chen, L. (2015), "Forced vibration of surface foundation on multi-layered half space", *Struct. Eng. Mech.*, **54**(4), 623-648.
Chen, X., Birk, C. and Song, C.M. (2015), "Transient analysis of wave propagation in layered soil by using the scaled boundary finite element method", *Comput. Geotech.*, **63**, 1-12.
Davies, T.G. and Banerjee, P.K. (1978), "The displacement field due to a point load at the interface of a two layer elastic half-space", *Geotechnique*, **28**(1), 43-56.
Gilbert, F. and Backus, G.E. (1966), "Propagator matrices in elastic wave and vibration problems", *Geophys.*, **31**(2), 326-332.
Gao, Q., Zhong, W.X. and Howson, W.P. (2004), "A precise method for solving wave propagation problems in layered anisotropic media", *Wave Motion*, **40**,191-207.
Genes, M.C. and Kocak, S. (2005), "Dynamic soil-structure interaction analysis of layered unbounded media via a coupled finite element/boundary element/scaled boundary finite element model", *Int. J. Numer. Meth. Eng.*, **62**(6), 798-823.
Harding, J.W. and Sneddon, I.N. (1945), "The elastic stresses produced by the indentation of the plane surface of a semi-infinite elastic solid by a rigid punch", *Math. Pr. Cambridge Philos. Soc.*, **41**(01), 16-26.
Kausel, E. and Peek, R. (1982), "Dynamic loads in the interior of a layered stratum: an explicit solution", *Bull. Seismol. Soc. Am.*, **72**(5), 1459-1481.
Kawana, F., Horiuchi, S., Terada, M., Kubo, K. and Matsui, K. (2012), "Theoretical solution based on volumetric strain of elastic multi layered structures under axisymmetrically distributed load", *J. JPN Soc. Civil Eng., Ser. E1 (Pav. Eng.)*, **68**(3), 383-394.
Kelvin, L. (1848), "Note on the integration of the equations of equilibrium of an elastic solid", *Cambridge Dublin Math. J.*, **3**, 87-89.
Khojasteh, A., Rahimian, M., Eskandari, M. and Pak, R.Y.S. (2008), "Asymmetric wave propagation in a transversely isotropic half-space in displacement potentials", *Int. J. Eng. Sci.*, **46**(7), 690-710.
Lamb, H. (1901), "On Boussinesq's problem", *Pr. London Math. Soc.*, **1**(1), 276-284.
Lin, G., Han, Z.J., Zhong, H. and Li, J.B. (2013), "A precise integration approach for dynamic impedance of rigid strip footing on arbitrary anisotropic layered half-space", *Soil Dyn. Earthq. Eng.*, **49**, 96-108.
Lin, G., Han, Z.J. and Li, J.B. (2013), "An efficient approach for dynamic impedance of surface footing on layered half-space", *Soil Dyn. Earthq. Eng.*, **49**, 39-51.
Lin, G., Han, Z.J. and Li, J.B. (2015), "General formulation and solution procedure for harmonic response of rigid foundation on isotropic as well as anisotropic multilayered half-space", *Soil Dyn. Earthq. Eng.*, **70**, 48-59.
Lu, S., Liu, J., Lin, G. and Wang, W.W. (2015), "Time-domain analyses of the layered soil by the modified scaled boundary finite element method", *Struct. Eng. Mech.*, **54**(5), 1055-1086.
Luco, J.E., Apsel, R.J. (1983), "On the Green's functions for a layered half-space. Part I", *Bull. Seismol. Soc. Am.*, **73**(4), 909-929.
Mindlin, R.D. (1936), "Force at a point in the interior of a semi-infinite solid", *J. Appl. Phys.*, **7**(5), 195-202.
Muki, R. (1960), "Asymmetric problems of the theory of elasticity for a semi-infinite solid and a thick plate", *Prog. Solid Mech.*, **1**, 401-439.
Nat, R.G., Sarva, J.S. and Sunita, R. (1992), "Static deformation of a stratified medium by general surface loads", *Indian J. Pure Appl. Math.*, **23**(9), 675-692.

Plevako, V.P. (1969), "A point force inside a pair of cohering half-spaces", *Soil Mech. Found. Eng.*, **6**(3), 165-169.
Rongved, L. (1955), "Force interior to one of two joined semi-infinite solids", *Proceedings of the Second Midwestern Conference on Solid Mechanics*, Lafayette, USA, September.
Selvadurai, A.P.S. (2001), "On Boussinesq's problem", *Int. J. Eng. Sci.*, **39**(3), 317-322.
Sneddon, I.N. (1951), *Fourier Transforms*, McGraw-Hill, New York, NY, USA.
Sneddon, I.N. (1972), *The Use Of Integral Transforms*, McGraw-Hill, New York, NY, USA.
Song, C.M. and Wolf, J.P. (1997), "The scaled boundary finite-element method-alias consistent infinitesimal finite-element cell method-for elastodynamics", *Comput. Meth. Appl. Mech. Eng.*, **147**, 329-355.
Stolle, D.F.E. (1989), "Axisymmetric analysis of multilayered media", *Eng. Anal. Bound. Elem.*, **6**(3), 118-122.
Wang, W. and Ishikawa, H. (2001), "A method for linear elasto-static analysis of multi-layered axisymmetrical bodies using Hankel's transform", *Comput. Mech.*, **27**(6), 474-483.
Wolf, J.P. and Song, C.M. (2000), "The scaled boundary finite-element method-a primer: derivations", *Comput. Struct.*, **78**(1), 191-210.
Wolf, J.P. (2003), *The Scaled Boundary Finite Element Method*, John Wiley & Sons, Chichester, WS, UK.
Yue, Z.Q. (1995), "On generalized Kelvin solutions in a multilayered elastic medium", *J. Elast.*, **40**(1), 1-43.
Yue, Z.Q. (1995), "Elastic fields in two joined transversely isotropic solids due to concentrated forces", *Int. J. Eng. Sci.*, **33**(3), 351-369.
Yue, Z.Q., Yin, J.H. and Zhang, S.Y. (1999), "Computation of point load solutions for geo-materials exhibiting elastic non-homogeneity with depth", *Comput. Geotech.*, **25**(2), 75-105.
Zhang, Z. and Li, Z. (2011), "Analytical solutions for the layered geo-materials subjected to an arbitrary point load in the cartesian coordinate", *Acta Mechanica Solida Sinica*, **24**(3), 262-272.
Zhong, W.X., Lin, J.H. and Gao, Q. (2004), "The precise computation for wave propagation in stratified materials", *Int. J. Numer. Meth. Eng.*, **60**(1), 11-25.
Zhong, W.X., Williams, F.W. and Bennett, P.N. (1997), "Extension of the Wittrick-Williams algorithm to mixed variable", *J. Vib. Acoust.*, **119**, 334-340.

CC